Location-Aided MmWave Hybrid Precoding Prediction for Air-to-Air Communications

Yipai Yan, Honglin Zhao(✉), Chengzhao Shan, Jiayan Zhang, and Yongkui Ma

School of Electronics and Information Engineering, Harbin Institute of Technology, Harbin 150001, China
hlzhao@hit.edu.cn

Abstract. Air-to-air (A2A) communications have been considered as one of the promising technologies to support various applications in future wireless communications, and high data rates are important for these applications such as aerial reconnaissance, remote sensing, and so on. However, it becomes unstable to provide high data rates services when suffering from the high mobility and huge path loss in A2A communications. Millimeter wave (mmWave) and massive MIMO precoding have been studied to meet the requirements of ever-increasing data rates. Unfortunately, MIMO full-digital precoding is considered by most of these methods, which leads to high complexity and power consumption. And the hybrid precoding is an efficient method to overcome this difficulty. Nevertheless, high relative velocity and long distance transmission are not taken into account in these researches. The objective of this paper is to develop an effective mmWave massive MIMO hybrid precoding strategy for high mobility and long distance communications. First, the A2A system is constructed and the evolution channel is derived. Second, a location-aided two-stage hybrid precoding prediction strategy is proposed. Moreover, the data transmission process of the system is discussed. Finally, numerical results manifest that the proposed strategy can effectively provide high data rates for A2A wireless communications.

Keywords: MmWave · Hybrid precoding · High mobility · A2A communications

1 Introduction

The dramatically growing demand for high data rates services, such as remoting sensing, disaster warnings, aerial photography and so on, has promoted the A2A communications attract much attention [1–3]. However, the A2A communications always need long range data transmission and are accompanied by the high relative velocity between the transceivers [4], which results in poor communication quality due to the significant path loss and high mobility. Millimeter wave (mmWave) and massive multiple-input-multiple-output (MIMO) are deemed as reliable techniques to meet the demand for high data rates [5]. MmWave offers

Q. Guo et al. (Eds.): WiSATS 2021, LNICST 410, pp. 345–356, 2022.
https://doi.org/10.1007/978-3-030-93398-2_34

huge available frequency spectrum ranging from 30 GHz to 300 GHz. And massive MIMO provides new spatial degrees of freedom communication capacity [6]. Thanks to the small wavelength of mmWave signals, the use of large-scale antenna arrays can be realized, and massive MIMO beamforming provides great array gain to combat the severe path loss at mmWave bands [7,8].

However, mmWave is rarely employed in long distance outdoor communications because of its severe free space attenuation and absorption loss [9]. Nevertheless, [10] explains the diminishing influence of the non-line-of-sight (NLOS) signal as altitude increases. Therefore, with the large-scale antenna arrays, highly directional beamforming can compensate huge path loss of LOS channel at mmWave. Meanwhile, for the high mobility systems, most of the researches [11–13] take MIMO full-digital architecture into consideration. On the one hand, to achieve the optimal spectral efficiency (SE), perfect channel state information (CSI) is needed [14], while it is quite challenging to be obtained in practice. On the other hand, the directional beamforming is rarely considered and resulting in short channel coherence time [15] under high mobility scenarios. In addition, due to the high complexity and power consumption of full-digital architecture [16], it is unaffordable for A2A system with limited energy supply. To overcome the above problems, the hybrid precoding architecture [16,17] has been proposed where the number of RF chains is far less than the number of antennas. It can perform both low-dimensional digital signal processing and directional beamforming. Unfortunately, most of the existing studies [18,19] assume the relative velocity between the transmitter and receiver is low, and the range of communication is short, which may not hold in A2A system.

In this paper, a novel hybrid precoding strategy is proposed to enhance SE in A2A wireless communications. First, the evolution channel for directional beamforming is derived. Then the location-aided analog precoder and combiner are obtained. Moreover, the Neumann series is utilized to predict digital precoder. Furthermore, hybrid precoding data transmission process is presented.

The remainder of this paper is organized as follows. In Sect. 2, an A2A system model and channel model for long distance mmWave communication are constructed, and some preliminaries of channel coherence time are revisited. In Sect. 3, a novel two-stage location-aided hybrid precoding prediction strategy is proposed, and data transmission process of the A2A system is also discussed. In Sect. 4, the performance of the proposed strategy is evaluated via simulations. Conclusions are drawn in Sect. 5.

We use the following notation throughout this paper: $\mathbf{A}^H$, $\mathbf{A}^{-1}$, $tr(\mathbf{A})$, $\|\mathbf{A}\|_F$ are the Hermitian, inverse, trace, Frobenius norm of the matrix $\mathbf{A}$; diag($\mathbf{a}$) is a diagonal matrix with the entries of $\mathbf{a}$ on its diagonal, blkdiag($\mathbf{a}_1, \ldots, \mathbf{a}_k$) is a block diagonal matrix with $\mathbf{a}_i$ is on its diagonal blocks.

2 System Model and Channel Model

2.1 System Model

We consider a mmWave massive MIMO A2A wireless system, as shown in Fig. 1, which consists of one control center and K mobile nodes. The altitude of control

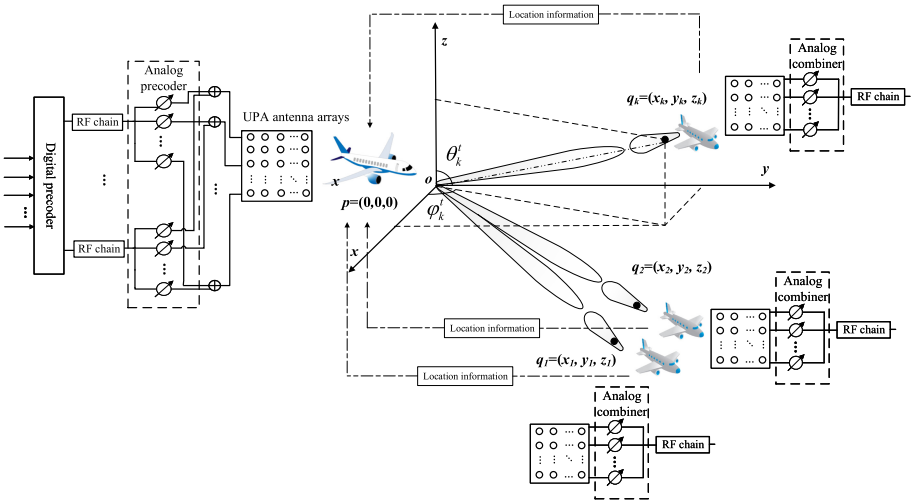

Fig. 1. A2A system model with hybrid precoding architecture.

is 3 km and mobile node is 8 km, and the relative velocity between control center and each mobile node is 300 m/s. It is assumed that the location information of the control center is $p = (0, 0, 0)$, and the location information of k-th mobile node is $q_k = (x_k, y_k, z_k)$. For control center, we assume a fully-connected architecture and it is equipped with K RF chains and $N_t = N_t^h \times N_t^v$ antennas, where $K \ll N_t$, while each mobile node is equipped with $N_r = N_r^h \times N_r^v$ antennas and has only one RF chain due to the limitation of energy supply. They both equipped with $\lambda/2$ spaced uniform planar array (UPA), N_t^h, N_t^v, N_r^h, and N_r^v are the number of antennas in horizontal and vertical directions for control center and each mobile node, respectively.

The transmitted symbols $\mathbf{s} \in \mathbb{C}^K$ with $\mathbb{E}\left[\mathbf{s}\mathbf{s}^H\right] = \mathbf{I}_K$ are first processed by a digital precoder $\mathbf{F}_{BB}$, then up-converted to RF domain and are processed with analog precoder $\mathbf{F}_{RF}$. With the k-th mobile node employs analog combiner $\mathbf{w}_{RF,k}$, the received signal at k-th mobile node is written as

$$y_k = \mathbf{w}_{RF,k}^H \mathbf{h}_k \mathbf{F}_{RF} \mathbf{F}_{BB} \mathbf{s} + \mathbf{w}_{RF,k}^H \mathbf{n}_k \tag{1}$$

where $\mathbf{h}_k$ is the channel matrix of k-th mobile node, $\mathbf{n}_k \in \mathbb{C}^{N_r}$ is the noise vector with $\mathcal{CN}\left(0, \sigma^2\right)$ entries.

The spectral efficiency at k-th mobile node is expressed as

$$R_k = \log_2(1 + \frac{\left|\mathbf{w}_{RF.k}^H \mathbf{h}_k \mathbf{F}_{RF} \mathbf{f}_{BB,k}\right|^2}{\sum_{i=1, i \neq k}^{K} \mathbf{w}_{RF.k}^H \mathbf{h}_k \mathbf{F}_{RF} \mathbf{f}_{BB,i} + \frac{\sigma^2 K}{P_t}}) \tag{2}$$

where P_t is the transmit power for per mobile node. To maximize the SE of the system, the objective function can be formulated as

$$\begin{aligned}(\mathbf{F}_{RF}, \mathbf{F}_{BB}) = &\underset{\mathbf{F}_{RF}, \mathbf{F}_{BB}}{\arg\max} \sum_{k=1}^{K} R_k \\ &s.t. \left|\mathbf{F}_{RF}(m,n)\right| = 1 \quad \forall m, n, \\ &\left\|\mathbf{F}_{RF}\mathbf{F}_{BB}\right\|_F^2 = K.\end{aligned} \tag{3}$$

2.2 Channel Model

For high elevation and long distance communication, the mmWave A2A channel will consist of LOS propagation and few NLOS components [20]. The channel vector of the k-th mobile node at m-th time slot is modeled as

$$\mathbf{h}_{m,k} = \sqrt{N_t N_r}\alpha_{m,k} e^{j2\pi f_d m T_c} \mathbf{a_r}(\varphi^r_{m,k}, \theta^r_{m,k}) \mathbf{a}_t^H(\varphi^t_{m,k}, \theta^t_{m,k}) \tag{4}$$

where $\alpha_{m,k}$ denotes the path gain, φ^t_k, θ^t_k, φ^r_k, θ^r_k, are azimuth angle of departure (AAoD), elevation angle of departure (EAoD), azimuth angle of arrival (AAoA), and elevation angle of arrival (EAoA), respectively. T_c is the symbol duration, f_d is the doppler shift, defined as

$$f_d = \mathbf{\Psi}^T \mathbf{f}_{d\max} \tag{5}$$

where $\mathbf{\Psi}$ is the spherical unit vector with φ^r_k and θ^r_k, defined as

$$\mathbf{\Psi} = [\sin\theta^r_k \cos\phi^r_k, \sin\theta^r_k \cos\phi^r_k, \cos\theta^r_k]^T \tag{6}$$

where $\mathbf{f}_{d\max}$ denotes the mobile node velocity vector and is given by

$$\mathbf{f}_{d\max} = \frac{v_k}{\lambda}[\sin\theta_{k,v}\cos\phi_{k,v}, \sin\theta_{k,v}\sin\phi_{k,v}, \cos\theta_{k,v}]^T \tag{7}$$

where v_k is the velocity of k-th mobile node, $\phi_{k,v}$ and $\theta_{k,v}$ denote the azimuth angle and elevation angle of travel direction, respectively. The array steering vector $\mathbf{a}(\varphi, \theta)$ is expressed as

$$\begin{aligned}\mathbf{a}(\varphi,\theta) &= \mathbf{a}_v(\varphi,\theta) \otimes \mathbf{a}_h(\varphi,\theta) \\ \mathbf{a}_v(\varphi,\theta) &= \frac{1}{\sqrt{N_v}}\left[1, \ldots, e^{j\pi(N_v-1)\cos\theta}\right]^T \\ \mathbf{a}_h(\varphi,\theta) &= \frac{1}{\sqrt{N_h}}\left[1, \ldots, e^{j\pi(N_h-1)\sin\theta\cos\varphi}\right]^T\end{aligned} \tag{8}$$

where N_v, N_h are the number of antennas in horizontal and vertical directions.

2.3 Temporal Correlations of the Channel

We assume perfect carrier and frame synchronization, and the effects of doppler have been mitigated by doppler pre-compensation process. The channel matrix at m-th time slot $\mathbf{H}_m$ is expressed as

$$\begin{aligned}
\mathbf{H}_m &= \sqrt{N_t N_r}\mathbf{A}_r\left(\varphi_m^r, \theta_m^r\right)\boldsymbol{\alpha}_m\mathbf{A}_t^H\left(\varphi_m^t, \theta_m^t\right) \\
\boldsymbol{\alpha}_m &= \mathrm{diag}\left(\alpha_{m,1}, \ldots, \alpha_{m,K}\right) \\
\mathbf{A}_r\left(\varphi_m^r, \theta_m^r\right) &= \mathrm{blkdiag}\left[\mathbf{a}_r\left(\varphi_{m,1}^{\mathrm{r}}, \theta_{m,1}^{\mathrm{r}}\right), \ldots, \mathbf{a}_r\left(\varphi_{m,K}^r, \theta_{m,K}^r\right)\right] \\
\mathbf{A}_t\left(\varphi_m^t, \theta_m^t\right) &= \left[\mathbf{a}_t\left(\varphi_{m,1}^t, \theta_{m,1}^t\right), \ldots, \mathbf{a}_t\left(\varphi_{m,K}^t, \theta_{m,K}^t\right)\right]
\end{aligned} \tag{9}$$

The channel matrix at $(m+1)$-th time slot $\mathbf{H}_{m+1}$ is expressed as

$$\mathbf{H}_{m+1} = \sqrt{N_t N_r}\mathbf{A}_r\left(\varphi_{m+1}^r, \theta_{m+1}^r\right)\boldsymbol{\alpha}_{m+1}\mathbf{A}_t^H\left(\varphi_{m+1}^t, \theta_{m+1}^t\right) \tag{10}$$

$$\begin{aligned}
\boldsymbol{\alpha}_{m+1} &= \boldsymbol{\alpha}_m + \sqrt{1-\epsilon^2}\mathbf{W}_m \\
\mathbf{A}_r\left(\varphi_{m+1}^r, \theta_{m+1}^r\right) &= \mathbf{A}_r\left(\varphi_m^r + \Delta\varphi_m^r, \theta_m^r + \Delta\theta_m^r\right) \\
\mathbf{A}_t\left(\varphi_{m+1}^t, \theta_{m+1}^t\right) &= \mathbf{A}_t\left(\varphi_m^t + \Delta\varphi_m^t, \theta_m^t + \Delta\theta_m^t\right)
\end{aligned} \tag{11}$$

where $\epsilon \in [0,1]$ is the channel correlation coefficient, and it is defined as [15]

$$\epsilon = \mathbb{E}\left[h_m h_{m+T_c}^*\right] = \int_{-\pi}^{\pi} e^{j2\pi f_d T_c} p\left(\alpha\right) \mathrm{d}\alpha \tag{12}$$

where the power angular spectrum (PAS) $p\left(\alpha\right)$ is normalized as $\int_{-\pi}^{\pi} p\left(\alpha\right) \mathrm{d}\alpha = 1$, α is the angle of incidence. For omnidirectional transmission, $p\left(\alpha\right) = (1/2\pi)$, while for directional beamforming, PAS can be modeled by a von Mises distribution function [15], the channel correlation coefficient becomes

$$\epsilon = \sqrt[4]{\frac{1}{\left(\frac{2\pi}{\lambda} v T_c \theta_b^2\right)^2 + 1}} \tag{13}$$

where θ_b is the beamwidth, λ is the signal wavelength.

$\mathbf{W}_m \in \mathbb{C}^{K\times K}$ denotes the additive white Gaussian noise with zero mean and unit variance, it is independent of $\boldsymbol{\alpha}_m$. $\Delta\varphi_m^t$, $\Delta\theta_m^t$, $\Delta\varphi_m^r$, $\Delta\theta_m^r$ are the angle variation of adjacent time slot in the direction of azimuth and elevation for AoD and AoA, respectively.

According to the Taylor expansion of the two variable functions, the matrix $\mathbf{A}_r\left(\varphi_m^r + \Delta\varphi_m^r, \theta_m^r + \Delta\theta_m^r\right)$ in (11) can be expressed as

$$\begin{aligned}
&\mathbf{A}_r\left(\varphi_m^r + \Delta\varphi_m^r, \theta_m^r + \Delta\theta_m^r\right) \\
&= \mathbf{A}_r\left(\varphi_m^r, \theta_m^r\right) + \left(\Delta\varphi_m^r \frac{\partial}{\partial\varphi_m^r} + \Delta\theta_m^r \frac{\partial}{\partial\theta_m^r}\right)\mathbf{A}_r\left(\varphi_m^r, \theta_m^r\right) \\
&+ \frac{1}{2!}\left(\Delta\varphi_m^r \frac{\partial}{\partial\varphi_m^r}\Delta\theta_m^r \frac{\partial}{\partial\theta_m^r}\right)^2 \mathbf{A}_r\left(\varphi_m^r, \theta_m^r\right) + \mathbf{R}_n
\end{aligned} \tag{14}$$

$\mathbf{A}_t\left(\varphi_m^t + \Delta\varphi_m^t, \theta_m^t + \Delta\theta_m^t\right)$ can be obtained by the similar way, which is omitted here.

For long distance A2A wireless communication, in a short time interval, $\Delta\varphi$ and $\Delta\theta$ are small [4], therefore, reserving the first term in (14), and other terms can be ignored. Then (14) can be rewritten as

$$\begin{aligned} \mathbf{A}_r\left(\varphi_m^r + \Delta\varphi_m^r, \theta_m^r + \Delta\theta_m^r\right) &\approx \mathbf{A}_r\left(\varphi_m^r, \theta_m^r\right) \\ \mathbf{A}_t\left(\varphi_m^t + \Delta\varphi_m^t, \theta_m^t + \Delta\theta_m^t\right) &\approx \mathbf{A}_t\left(\varphi_m^t, \theta_m^t\right) \end{aligned} \tag{15}$$

Combining (10), (11) and (15) yields

$$\begin{aligned} \mathbf{H}_{m+1} &= \epsilon\mathbf{H}_m + \sqrt{1-\epsilon^2}\mathbf{N}_m \\ \mathbf{N}_m &= \sqrt{N_t N_r}\mathbf{A}_r\left(\varphi_m^r, \theta_m^r\right)\mathbf{W}_m\mathbf{A}_t^H\left(\varphi_m^t, \theta_m^t\right) \end{aligned} \tag{16}$$

The following derivations are based on the evolution channel model in (16), and a more efficient hybrid precoding prediction strategy, which can exploit the temporal correlation of (16), is proposed for mmWave A2A system.

3 Two-Stage Hybrid Precoding Prediction Design for A2A Communications

In this section, a novel two-stage hybrid precoding strategy is presented for the system in Fig. 1. The proposed strategy leverages the channel correlation to maximize the spectral efficiency with reduced complexity.

3.1 Analog Precoder and Combiner Design

For long distance A2A communications, as discussed above, only LOS transmission is considered. Based on the geometrical relationship as illustrated in Fig. 1, AAoD and EAoD can be performed as

$$\begin{aligned} \varphi_k^t &= \arctan\left(\frac{y_k}{x_k}\right) \\ \theta_k^t &= \arctan\left(\frac{\sqrt{x_k^2 + y_k^2}}{z_k}\right) \end{aligned} \tag{17}$$

φ_k^r and θ_k^r can be obtained by the similar way, which is omitted here.

It is assumed that the phase-only controlled phase shifter is employed, and we match the analog precoder and combiner with array steering vector and array response vector, respectively. For the given direction φ_k^t, θ_k^t, φ_k^r, θ_k^r, the ideal analog precoder and combiner of the k-th mobile node are formulated as

$$\begin{aligned} \mathbf{f}_{RF,k} &= \mathbf{a}_t(\varphi_k^t, \theta_k^t) \\ \mathbf{w}_{RF,k} &= \mathbf{a}_r(\varphi_k^r, \theta_k^r) \end{aligned} \tag{18}$$

We define the beam update period (BUP) T_b as the location information update time. At n-th BUP, location and relative velocity for the k-th user is

$$\begin{aligned} q_{n,k} &= (x_{n,k}, y_{n,k}, z_{n,k}) \\ v_{n,k} &= (v_{x_{n,k}}, v_{y_{n,k}}, v_{z_{n,k}}) \end{aligned} \tag{19}$$

It is assumed that the mobile node is moving uniformly and in a straight line during one BUP. The location information of $(n+1)$-th beam update period $q_{n+1,k} = (x_{n+1,k}, y_{n+1,k}, z_{n+1,k})$ can be written as

$$\begin{aligned} x_{n+1,k} &= x_{n,k} + T_b \cdot v_{x_{n,k}} \\ y_{n+1,k} &= y_{n,k} + T_b \cdot v_{y_{n,k}} \\ z_{n+1,k} &= z_{n,k} + T_b \cdot v_{z_{n,k}} \end{aligned} \tag{20}$$

Moreover, AoA and AoD of $(n+1)$-th BUP are obtained depending on (17).

3.2 Digital Precoder Design

Since the mobile nodes are not separated, there exists interference among data streams. Therefore, zero-forcing (ZF) approach to eliminate interference based on equivalent baseband channel is considered. We have the equivalent baseband channel matrix $\mathbf{H}_{eq}$ as follows

$$\mathbf{H}_{eq} = \mathbf{W}_{RF}^{H} \mathbf{H} \mathbf{F}_{RF} \tag{21}$$

where $\mathbf{F}_{RF} = [\mathbf{f}_{RF,1}, \mathbf{f}_{RF,2}, \ldots, \mathbf{f}_{RF,K}]$, $\mathbf{W}_{RF} = \text{blkdiag}[\mathbf{w}_{RF,1}, \mathbf{w}_{RF,2}, \ldots, \mathbf{w}_{RF,K}]$.

As mentioned above, $\mathbf{H}_{eq}$ is a low dimensional square matrix. We define the channel update period (CUP, also called time slot) T_c as the equivalent channel update time. The ZF digital precoder of $(m+1)$-th CUP is derived as

$$\mathbf{F}_{BB,m+1} = \mathbf{H}_{eq,m+1}^{-1} \tag{22}$$

In general, $\mathbf{H}_{eq}$ should be updated at each time slot to maintain the spectral efficiency. However, when the relative velocity is high, there is insufficient time for channel estimation. Fortunately, in terms of (16), the channels of adjacent time slot are correlated, thus the outdated equivalent CSI can be utilized to predict the digital precoder.

Combining (16), (21) and (22) leads to

$$\mathbf{F}_{BB,m+1} = \left(\epsilon \mathbf{H}_{eq,m} + \sqrt{1-\epsilon^2} \mathbf{W}_m \right)^{-1} \tag{23}$$

The inverse of the sum of two arbitrary matrices is generally difficult to split. In particular, as ϵ is large, noise matrix can be considered as a disturbance term. Turn to Neumann series [21], it provides approximations of the inverse of the sum of two matrices when one of the matrix has entries of small magnitude. Then (23) can be rewritten as

$$\begin{aligned} \mathbf{F}_{BB,m+1} &= \sum_{k=0}^{\infty} (-1)^k \left((\epsilon \mathbf{H}_{eq,m})^{-1} \sqrt{1-\epsilon^2} \mathbf{W}_m \right)^k (\epsilon \mathbf{H}_{eq,m})^{-1} \\ &= (\epsilon \mathbf{H}_{eq,m})^{-1} - \left((\epsilon \mathbf{H}_{eq,m})^{-1} \sqrt{1-\epsilon^2} \mathbf{W}_m \right) (\epsilon \mathbf{H}_{eq,m})^{-1} \\ &\quad + \left((\epsilon \mathbf{H}_{eq,m})^{-1} \sqrt{1-\epsilon^2} \mathbf{W}_m \right)^2 (\epsilon \mathbf{H}_{eq,m})^{-1} - \cdots \end{aligned} \tag{24}$$

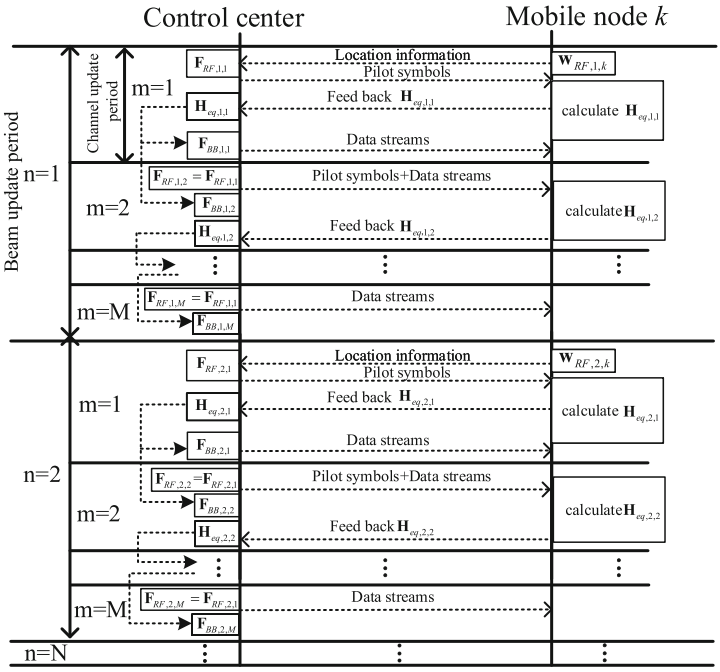

Fig. 2. Hybrid precoding data transmission process.

When ϵ is large enough, the first term in (24) is reserved, the following terms are ignored. The predictive digital precoder can be approximately written as

$$\widetilde{\mathbf{F}}_{BB,m+1} \approx (\epsilon \mathbf{H}_{eq,m})^{-1} \tag{25}$$

3.3 Hybrid Precoding Data Transmission Process

The definitions of BUP and CUP have been explained above, and it is assumed that one BUP contains several CUPs. The equivalent baseband channel almost unchanged within one CUP, but could vary for different CUP; AoA and AoD nearly do not vary in one BUP, they vary for different BUP. The steps involved in establishing a data transmission link during one BUP are summarized as follows:

- Step 1: At the initial CUP, each mobile node sends its location to the control center. Analog precoder and combiner are designed based on (17).
- Step 2: Control center transmits pilot symbols to calculate $\mathbf{H}_{eq}$.
- Step 3: $\mathbf{H}_{eq}$ is fed back to control center, then digital precoder is derived and data streams are transmitted to each mobile node.

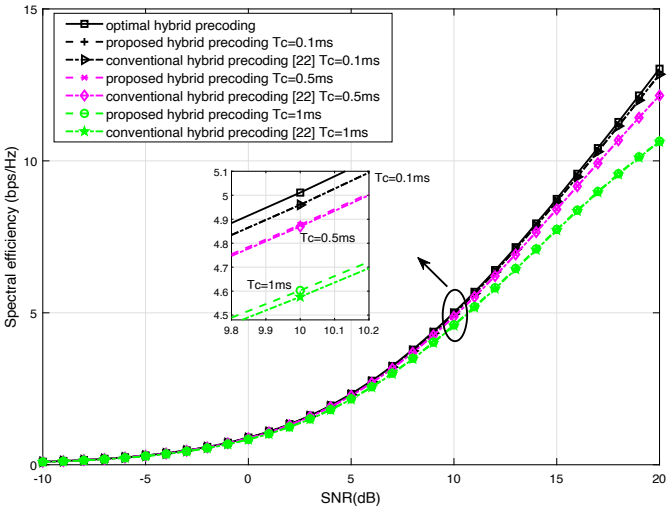

Fig. 3. Spectral efficiency versus SNR with different channel coherence time.

- Step 4: At the second CUP, analog precoder and combiner are unchanged, digital precoder is predicted according to (25). Then the pilot symbols and data streams are sent simultaneously by hybrid precoding. The pilot symbols are used to estimate the $\mathbf{H}_{eq}$ of current time slot.
- Step 5: $\mathbf{H}_{eq}$ of current time slot is fed back to control center to predict the digital precoder of next time slot.

Repeating step 4 to step 5 until the end of a BUP, and at the last CUP, only data streams need to be transfered. The details are shown in Fig. 2. For the second and subsequent BUP, if the mobile node moves uniformly in a straight line, location information does not need to be fed back, the analog precoder can be obtained according to (17) and (20). Otherwise, the location information should be fed back at the beginning of each BUP.

For conventional strategy [22], first the transmitter sends pilot symbols to estimate channel, then the receiver feeds back the estimated CSI to transmitter, next the precoder can be designed by transmitter to transmit data information. While for the proposed strategy, the channel estimation and data transmission are carried out together, thus the overhead of the system is considerably reduced.

4 Numerical Results

To confirm the validity of the derived digital precoder approximation in (25) and evaluate the performance of the proposed location-aided hybrid precoding strategy, we conduct simulations and discuss the numerical results in this section. We compare the proposed strategy to optimal strategy in (22) and the conventional strategy [22]. To provide a fair comparison, CSI is updated every BUP

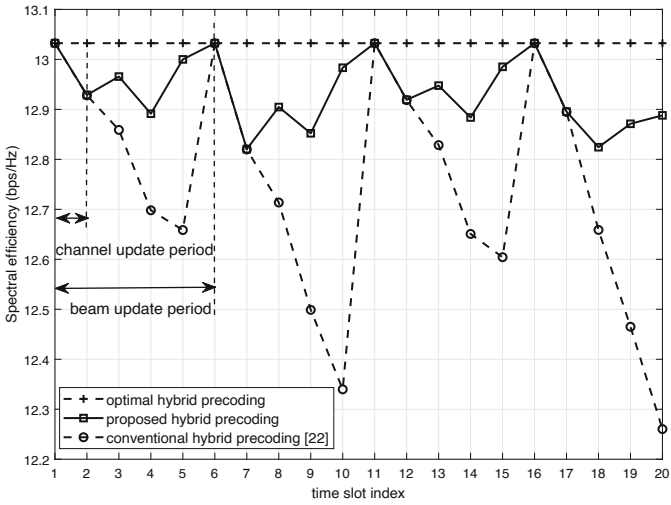

Fig. 4. Spectral efficiency versus time slot index with SNR = 20 dB and $T_c = 0.1$ ms.

for conventional strategy. We consider a mmWave massive MIMO system with carrier frequency $f_c = 30$ GHz where the control center is equipped with 64×64 UPA and each mobile node is equipped with 8×8 UPA. There are $K = 4$ mobile nodes. The initial distance between control center and mobile node is 44 km, 46 km, 47 km, 50 km, respectively, and the relative velocity is 300 m/s.

Figure 3 illustrates the spectral efficiency of the system with different channel coherence time versus SNR. As shown in Fig. 3, the SE of the proposed strategy is considerably close to the optimal hybrid precoding. As SNR goes large, a gap can be seen between the optimal strategy and the proposed strategy. In low SNR regime, the noise is the main influence for performance, while for high SNR regime, the interference between the data streams has a great impact on performance, residual interference due to approximation of Neumann series causes performance degradation. Figure 3 also shows that as channel coherence time becomes small, the proposed strategy approaches the optimal strategy closely. This is because the correlation between channel of adjacent time slot becomes stronger, thus the predicted precoder matrix has a smaller difference with the optimal precoder matrix. Therefore, we have to make a trade-off between SE and channel coherence time in practice. It can also be seen that the spectral efficiency of conventional strategy is close to the proposed strategy, the reason is that we only consider single time slot, without considering the influence of time on the performance.

Figure 4 depicts the spectral efficiency versus time slot index with different hybrid precoding strategy under the assumption that SNR = 20 dB, $T_c = 0.1$ ms. In simulation, 4 BUPs are considered here, and each BUP contains 5 CUPs. As shown in Fig. 4, the SE of the proposed strategy fluctuates under the optimal performance over time, in contrast, because of channel mismatch, the SE of

conventional strategy continues to degrade as time goes on during one BUP, until it updates CSI. It is obvious that the proposed strategy can still maintain high spectral efficiency in high mobility scenarios compared with the conventional strategy.

5 Conclusions

In this paper, we have developed a novel hybrid precoding strategy for A2A system to overcome the problem of CSI outdated in high mobility scenarios and huge path loss for long distance transmission. We first derived the evolution channel for mmWave A2A communication. Then a two-stage hybrid precoding prediction strategy was proposed while the analog precoder and combiner were obtained based on location information, and the digital precoder was derived according to Neumann series approximation. Moreover, data transmission process of the proposed strategy was presented. Finally, numerical results verified the proposed strategy can achieve high spectral efficiency for A2A mmWave wireless communications.

References

1. Liu, W., Zang, X., Li, Y., Vucetic, B.: Over-the-air computation systems: optimization, analysis and scaling laws. IEEE Trans. Wirel. Commun. **19**(8), 5488–5502 (2020). https://doi.org/10.1109/TWC.2020.2993703
2. Ma, Z., Ai, B., He, R., Wang, G., Niu, Y., Zhong, Z.: A wideband non-stationary air-to-air channel model for UAV communications. IEEE Trans. Veh. Technol. **69**(2), 1214–1226 (2020). https://doi.org/10.1109/TVT.2019.2961178
3. Bai, L., Han, R., Liu, J., Yu, Q., Choi, J., Zhang, W.: Air-to-ground wireless links for high-speed UAVs. IEEE J. Sel. Areas Commun. **38**(12), 2918–2930 (2020). https://doi.org/10.1109/JSAC.2020.3005471
4. Li, Y., Miridakis, N.I., Tsiftsis, T.A., Yang, G., Xia, M.: Air-to-air communications beyond 5G: a novel 3D CoMP transmission scheme. IEEE Trans. Wirel. Commun. **19**(11), 7324–7338 (2020). https://doi.org/10.1109/TWC.2020.3010569
5. Bogale, T.E., Le, L.B.: Massive MIMO and mmWave for 5G wireless HetNet: potential benefits and challenges. IEEE Veh. Technol. Mag. **11**(1), 64–75 (2016). https://doi.org/10.1109/MVT.2015.2496240
6. Björnson, E., Larsson, E.G., Marzetta, T.L.: Massive MIMO: ten myths and one critical question. IEEE Commun. Mag. **54**(2), 114–123 (2016). https://doi.org/10.1109/MCOM.2016.7402270
7. Shan, C., Ma, Y., Zhao, H., Shi, J.: Joint radar-communications design based on time modulated array. Digit. Signal Process. **82**, 43–53 (2018). https://doi.org/10.1016/j.dsp.2018.07.013
8. Shan, C., Ma, Y., Zhao, H., Shi, J.: Time modulated array sideband suppression for joint radar-communications system based on the differential evolution algorithm. Digit. Signal Process. **97**, 102601 (2020). https://doi.org/10.1016/j.dsp.2019.102601
9. Xiao, M., et al.: Millimeter wave communications for future mobile networks. IEEE J. Sel. Areas Commun. **35**(9), 1909–1935 (2017). https://doi.org/10.1109/JSAC.2017.2719924

10. Goddemeier, N., Wietfeld, C.: Investigation of air-to-air channel characteristics and a UAV specific extension to the rice model. In: 2015 IEEE Globecom Workshops (GC Wkshps), pp. 1–5 (2015). https://doi.org/10.1109/GLOCOMW.2015.7414180
11. Kim, K., Kim, T., Love, D.J., Kim, I.H.: Differential feedback in codebook-based multiuser MIMO systems in slowly varying channels. IEEE Trans. Commun. **60**(2), 578–588 (2012). https://doi.org/10.1109/TCOMM.2011.012012.110051
12. Kim, T., Love, D.J., Clerckx, B.: MIMO systems with limited rate differential feedback in slowly varying channels. IEEE Trans. Commun. **59**(4), 1175–1189 (2011). https://doi.org/10.1109/TCOMM.2011.022811.090744
13. Chen, H., Lin, Y.: Differential feedback of geometrical mean decomposition precoder for time-correlated MIMO systems. IEEE Trans. Signal Process. **65**(14), 3833–3845 (2017). https://doi.org/10.1109/TSP.2017.2692741
14. Ayach, O.E., Rajagopal, S., Abu-Surra, S., Pi, Z., Heath, R.W.: Spatially sparse precoding in millimeter wave MIMO systems. IEEE Trans. Wirel. Commun. **13**(3), 1499–1513 (2014). https://doi.org/10.1109/TWC.2014.011714.130846
15. Va, V., Choi, J., Heath, R.W.: The impact of beamwidth on temporal channel variation in vehicular channels and its implications. IEEE Trans. Veh. Technol. **66**(6), 5014–5029 (2017). https://doi.org/10.1109/TVT.2016.2622164
16. Kutty, S., Sen, D.: Beamforming for millimeter wave communications: an inclusive survey. IEEE Commun. Surv. Tutor. **18**(2), 949–973 (2016). https://doi.org/10.1109/COMST.2015.2504600
17. Ahmed, I., et al.: A survey on hybrid beamforming techniques in 5G: architecture and system model perspectives. IEEE Commun. Surv. Tutor. **20**(4), 3060–3097 (2018). https://doi.org/10.1109/COMST.2018.2843719
18. Liu, J., Bentley, E.S.: Hybrid-beamforming-based millimeter-wave cellular network optimization. IEEE J. Sel. Areas Commun. **37**(12), 2799–2813 (2019). https://doi.org/10.1109/JSAC.2019.2947923
19. Sun, S., Rappaport, T.S., Shafi, M., Tataria, H.: Analytical framework of hybrid beamforming in multi-cell millimeter-wave systems. IEEE Trans. Wirel. Commun. **17**(11), 7528–7543 (2018). https://doi.org/10.1109/TWC.2018.2868096
20. Cuvelier, T., Heath, R.W.: MmWave MU-MIMO for aerial networks. In: 2018 15th International Symposium on Wireless Communication Systems (ISWCS), pp. 1–6 (2018). https://doi.org/10.1109/ISWCS.2018.8491045
21. Meyer, C.D.: Matrix Analysis and Applied Linear Algebra. Society for Industrial and Applied Mathematics (2000)
22. Zhou, S., Xu, W., Zhang, H., You, X.: Hybrid precoding for millimeter wave massive MIMO with analog combining. In: 2017 9th International Conference on Wireless Communications and Signal Processing (WCSP), pp. 1–5 (2017). https://doi.org/10.1109/WCSP.2017.8171060